JACS
JOURNAL OF THE AMERICAN CHEMICAL SOCIETY
Article
pubs.acs.org/JACS

Tunable Biomimetic Chalcogels with Fe_4S_4 Cores and $[Sn_nS_{2n+2}]^{4-}$ (n = 1, 2, 4) Building Blocks for Solar Fuel Catalysis

Yurina Shim,[†] Benjamin D. Yuhas,[†] Scott M. Dyar,[†] Amanda L. Smeigh,[†] Alexios P. Douvalis,[‡] Michael R. Wasielewski,[†] and Mercouri G. Kanatzidis*[,†]

[†]Department of Chemistry and Argonne-Northwestern Solar Energy Research (ANSER) Center, Northwestern University, Evanston, Illinois 60208, United States

[‡]Department of Physics, University of Ioannina, 45110 Ioannina, Greece

Supporting Information

ABSTRACT: Biology sustains itself by converting solar energy in a series of reactions between light harvesting components, electron transfer pathways, and redox-active centers. As an artificial system mimicking such solar energy conversion, porous chalcogenide aerogels (chalcogels) encompass the above components into a common architecture. We present here the ability to tune the redox properties of chalcogel frameworks containing biological Fe_4S_4 clusters. We have investigated the effects of $[Sn_nS_{2n+2}]^{4-}$ linking blocks ($[SnS_4]^{4-}$, $[Sn_2S_6]^{4-}$, $[Sn_4S_{10}]^{4-}$) on the electrochemical and electrocatalytic properties of the chalcogels, as well as on the photophysical properties of incorporated light-harvesting dyes, tris(2,2′-bipyridyl)ruthenium(II) ($Ru(bpy)_3^{2+}$). The various thiostannate linking blocks do not alter significantly the chalcogel surface area (90−310 m^2/g) or the local environment around the Fe_4S_4 clusters as indicated by ^{57}Fe Mössbauer spectroscopy. However, the varying charge density of the linking blocks greatly affects the reduction potential of the Fe_4S_4 cluster and the electronic interaction between the clusters. We find that when the Fe_4S_4 clusters are bridged with the adamantane $[Sn_4S_{10}]^{4-}$ linking blocks, the electrochemical reduction of CS_2 and the photochemical production of hydrogen are enhanced. The ability to tune the redox properties of biomimetic chalcogels presents a novel avenue to control the function of multifunctional chalcogels for a wide range of electrochemical or photochemical processes relevant to solar fuels.

INTRODUCTION

The motivation to develop alternative energy sources that are clean, abundant and renewable has directed great attention to understanding the science and mimicking the function of natural photosynthesis.[1−4] Natural photosynthesis has converted solar energy to stored chemical energy to maintain the diversity of living organisms for more than 3 billion years.[5−7] An intense research effort is focused on simplifying natural photosynthesis while integrating the core reaction centers in a common structural system to achieve similar results to those found in nature.[8−15] For example, the chemistry of cubane Fe_4S_4 clusters, which are ubiquitous in nature, has developed into a mature research area with various analogous inorganic and organometallic molecules.[16−24] In nature, Fe_4S_4 clusters are involved in redox processes such as photosynthesis, nitrogen fixation, and respiration,[25] and frequently found in both electron pathways and in active sites of metalloenzymes.[19,20,26−28] They are electron carriers in some enzymes such as ferredoxin, hydrogenase, and nitrogenase, and compose active sites in others including sulfite reductase, [FeFe] hydrogenase, and acetyl coenzyme A synthase.[27,29−31] In natural enzymes, the active Fe_4S_4 clusters are often coordinated in highly evolved systems with complex biochemical pathways to perform their catalytic and electron-transferring functions.[16,27,32,33]

To simplify the complicated biological assemblies, various analogue molecules have been developed and some synthetic clusters have shown catalytic capability in a designed environment,[34−37] including the ability to produce hydrogen photochemically.[38] Expanding to other iron sulfur molecules, many reports have been also published on diiron analogue molecules concerning hydrogen-producing ability.[39−45] Though many of these molecules have been shown to catalyze hydrogen production from water, in general the catalytic function of these synthetic molecules is deactivated by the presence of oxygen and the undesirable products of water-splitting reaction.[39,46,47] An emerging strategy for increasing the long-term stability of the catalysts is to embed them into a larger framework, mimicking the catalytic sites in natural enzymes. We have sought the incorporation of Fe_4S_4 clusters in a larger structure as a promising approach to stabilize them and protect them from deactivating side reactions.

Received: November 17, 2012
Published: January 31, 2013

   dx.doi.org/10.1021/ja311310k | J. Am. Chem. Soc. 2013, 135, 2330−2337

Table 1. Synthetic Parameters and the Empirical Formula of Chalcogels before and after Functionalization with $Ru(bpy)_3Cl_2$, and after Washing with Pure Ethanol, Calculated by the Elemental Amounts Determined by EDS Spectroscopy

aerogel	ITS-cg1 ($[SnS_4]$)	ITS-cg2 ($[Sn_2S_6]$)	ITS-cg3 ($[Sn_4S_{10}]$)
$[Fe_4S_4]$ (mmol)	0.125	0.1	0.1
$[Sn_xS_{2x+2}]^{4-}$ (mmol)	0.1	0.1	0.1
Observed Empirical Formula	$Na_{2.1}P_{0.9}[Fe_4S_4]_{1.7}[SnS_4]_2$	$Na_{2.2}P_{1.1}[Fe_4S_4]_{1.5}[Sn_2S_6]_2$	$P_{2.4}[Fe_4S_4]_{3.1}[Sn_4S_{10}]_2$
After functionalization	$Ru_{1.5}[Fe_4S_4]_{1.4}[SnS_4]_2Cl_{1.6}$	$Ru_{1.7}[Fe_4S_4]_{1.5}[Sn_2S_6]_2Cl_{1.5}$	$Ru_{3.3}[Fe_4S_4]_{3.0}[Sn_4S_{10}]_2Cl_{2.2}$
After wash	$Ru_{1.4}[Fe_4S_4]_{1.4}[SnS_4]_2Cl_{1.0}$	$Ru_{1.3}[Fe_4S_4]_{1.3}[Sn_2S_6]_2Cl_{1.0}$	$Ru_{3.3}[Fe_4S_4]_{3.0}[Sn_4S_{10}]_2Cl_{1.7}$

[a]P: represents the Ph_4P cation.

We have recently introduced a new class of porous chalcogenide aerogels, called *chalcogels*, that can be functionalized with biomimetic functionalities.[48,49] These chalcogels are functionalized with light harvesting components, electron transfer pathways, and redox-active centers all into one suprastructure.[48−50] These biomimetic chalcogels utilize redox-active $[Fe_4S_4]^{2+}$ cluster units linked by $[Sn_2S_6]^{4-}$ building blocks to form polymeric extended structures. This new type of chalcogels has been shown to reduce protons electrocatalytically and photochemically with retained redox activity of the Fe_4S_4 cluster.

In an effort to control the electrochemical properties of the multifunctional chalcogels, we explore the tunability of our biomimetic chalcogels for a wider range of reactions relevant to solar fuels. It is especially challenging to adjust the redox properties of the Fe_4S_4 cluster both electrochemically and photochemically in a solid state system such as the chalcogel environment. Broadening the family of biomimetic chalcogels, here we studied a series of high surface area materials using the $[SnS_4]^{4-}$, $[Sn_2S_6]^{4-}$ and $[Sn_4S_{10}]^{4-}$ (referred to as the $[Sn_nSn_{2n+2}]^{4-}$ series) building blocks. We show that it is possible to control the relevant electrochemical redox potential of the Fe_4S_4 clusters by varying n and as a result enhance the light to hydrogen conversion capability shown by the dye-functionalized chalcogels, $\{[Fe_4S_4]_x[Sn_nSn_{2n+2}]_y[Ru(bpy)_3]_z\}$.

RESULTS AND DISCUSSION

The biomimetic chalcogels are chemically integrated materials that bring redox-catalytic active components close to light-harvesting photoredox components, which can facilitate electrochemical and photochemical reduction of various substrates.[48−50] Our relatively facile bottom-up synthetic method enables the variation of components that could be integrated into the system. This flexibility of chalcogel systems opens up the possibility of tuning the electrochemical and photochemical parameters of the biomimetic chalcogels tailored to the various light-driven reactions related to the solar fuel productions. Here, we show that the control of electrochemical energies of the Fe_4S_4 cluster can be easily achieved by utilizing the synthetic flexibility of the chalcogel system and by varying the size of the linking blocks. Previously we described multifunctional porous chalcogels based on $[Sn_2S_6]^{4-}$ as linking blocks of Fe_4S_4 cubane clusters, referring to them here as ITS-cg2. Here we expand the family of iron sulfur tin sulfide chalcogels (ITS-cg) with two additional thiostannate linking blocks. The linking units newly introduced here are the tetrahedral cluster $[SnS_4]^{4-}$ (ITS-cg1) and adamantane cluster $[Sn_4S_{10}]^{4-}$ (ITS-cg3). Other than molecular size, the key property difference between these three anions is the charge density which varies as $[SnS_4]^{4-} > [Sn_2S_6]^{4-} > [Sn_4S_{10}]^{4-}$. This trend defines the ligating ability of the thiostannate clusters to the Fe atoms of the Fe_4S_4 cluster and the degree of charge transfer to it. Furthermore, based on a simple packing argument the chalcogels featuring the small sized building blocks of $[SnS_4]^{4-}$ should have Fe_4S_4 clusters in closer average spatial proximity to one another compared to the chalcogels containing the significantly larger $[Sn_4S_{10}]^{4-}$ units. Here we study the effects of these linking blocks on the properties of chalcogels with Fe_4S_4 cubane centers.

The chalcogels were synthesized in a similar manner (Table 1) as ITS-cg2 with the aim to create anionic porous networks using the metathesis reaction as suggested by the equation:

$$\{[Fe_4S_4Cl_4]\}^{2-} + [Sn_nS_{2n+2}]^{4-} \rightarrow \{[Fe_4S_4]_x[Sn_nS_{2n+2}]_y\}^{z-} + yCl^-$$

The metathesis reaction between the tin sulfide precursor ($Na_4SnS_4{\cdot}14H_2O$ for ITS-cg1, $((CH_3CH_2)_4N)_4Sn_4S_{10}$ for ITS-cg3) and iron sulfide ($(Ph_4P)_2Fe_4S_4Cl_4$)[17,18] precursor results in polymerization that produces a porous solid gel as shown in Figure 1. The terminal chloride ligands on the iron sulfur cubane cluster are replaced by the sulfur atoms from the anionic tin sulfide clusters in the metathesis reaction (Scheme 1). In addition, the mononuclear and binuclear thiostannate anions potentially have the ability to chelate to a single Fe atom which previously has been shown to significantly raise its redox potential.[51] Both ITS-cg1 and ITS-cg3 display spongy, porous structures under electron microscopy and appear amorphous in TEM image and capillary X-ray diffraction experiments (Figures 1B,C, and 2A).

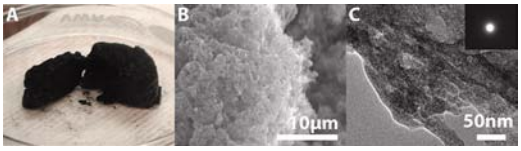

Figure 1. (A) Image of the sliced typical ITS-cg sample. (B) SEM image showing porous nature of ITS-cg sample. (C) TEM image showing porous and nonperiodic structure of ITS-cg sample. Inset is selected area e-beam diffraction showing only diffuse scattering.

The resulting chalcogel network is negatively charged overall, balanced by the counter-cations of the precursors such as Ph_4P^+, Na^+, or $[(CH_3CH_2)_4N]^+$. Elemental analysis of the chalcogels supports the existence of these counter-cations (Table 1, Figure 2B). The simple ion exchange reaction with Cs^+ ions displaces the counter-cations of the precursors (Ph_4P^+ and $[(CH_3CH_2)_4N]^+$) confirming the role of counter-cations as charge balancers in ITS-cg3 (Table 2, Figure 2C). Though the elements from $[(CH_3CH_2)_4N]^+$ cannot be detected under SEM/EDS, its existence is expected and might explain the excess amount of Cs^+ compared to the amount of P detected before the ion exchange. This ability to undergo simple ion

dx.doi.org/10.1021/ja311310k | J. Am. Chem. Soc. 2013, 135, 2330−2337

Scheme 1. Assembly of $[Fe_4S_4]^{2+}/[Sn_4S_{10}]^{4-}$ (ITS-cg3) and Functionalization of the Framework with Light-Harvesting Cations of $Ru(bpy)_3^{2+}$ (TEA represents $(CH_3CH_2)_4N$)

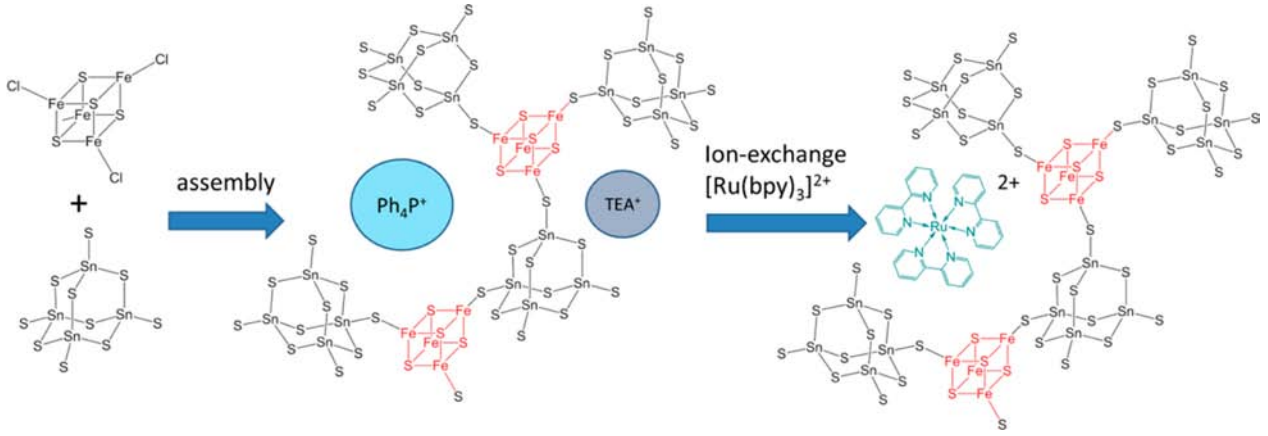

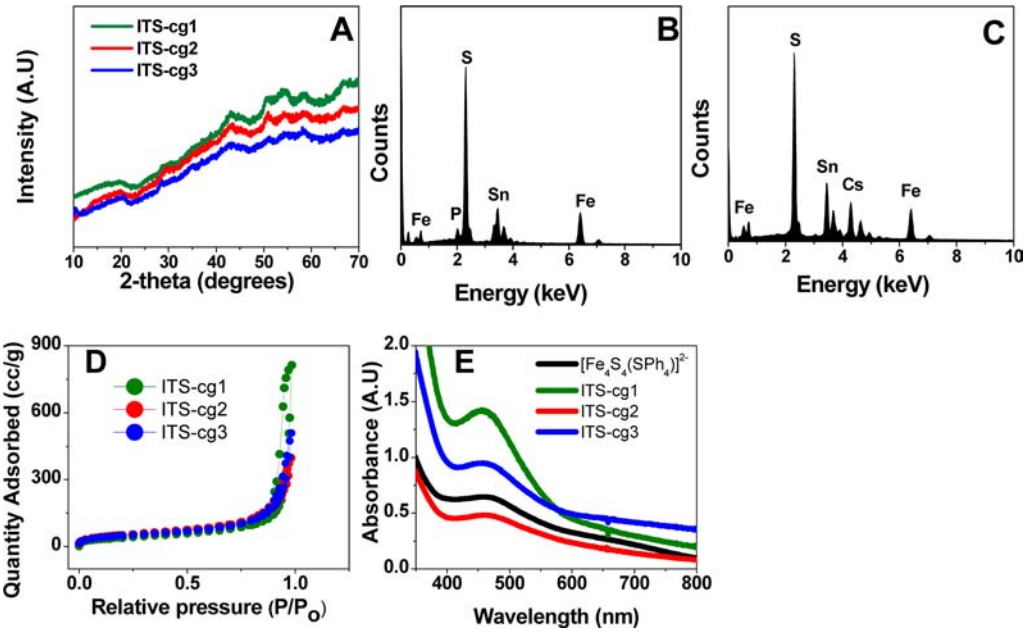

Figure 2. (A) Powder XRD patterns of ITS-cg1,2 and 3, illustrating the absence of an extended lattice structure for all three chalcogel samples. The rising background intensity at higher diffraction angles is due to the X-ray fluorescence of iron in the samples. (B and C) Typical EDS spectrum of ITS-cg3 before (B) and after ion exchange with CsCl (C) showing displacement of counter cations by Cs^+. (D) Nitrogen adsorption/desorption isotherm at 77K of chalcogels, exhibiting the mixture of meso and macro pore distribution. (E) UV−vis spectra of chalcogel solutions after thiol extrusion experiment, reflecting the absorption of the extruded $[Fe_4S_4(SPh_4)]^{2-}$ anion in all chalcogels.

Table 2. The Empirical Formula, Calculated from the Atomic % Obtained from Elemental Analysis, of ITS-cg3 before and after Ion Exchange with CsCl

observed empirical formula before	after
$P_{2.4}[Fe_4S_4]_{3.1}[Sn_4S_{10}]_2$	$Cs_{6.8}[Fe_4S_4]_{2.8}[Sn_4S_{10}]_2$

exchange is a key property because it enables the easy incorporation of light harvesting dye, tris(2,2′-bipyridyl)-ruthenium(II) ($Ru(bpy)_3^{2+}$), into the chalcogel framework, which will be discussed in detail later.

The porous high surface area structures of the chalcogels are characterized with a mixture of macropores and mesopores, exhibiting Type IIb behavior from the nitrogen adsorption isotherms regardless of linking unit (Figure 2D). The estimated surface areas of the aerogels range from 90 to 310 m^2/g for both ITS-cg1 and 3 similar to those of ITS-cg2.[48]

The incorporated Fe_4S_4 cluster inside the chalcogels were detected by UV−visible spectroscopy after thiol extrusion experiments, a well-established method of detecting Fe_4S_4 clusters in their native proteins.[52] When the excess thiophenol reacts with the chalcogels in *N*,*N*′-dimethylformamide, the thiol extrudes the Fe_4S_4 cluster from the chalcogel framework, resulting in a brown/black uniform solution. The uniform solution from both ITS-cg1 and 3 shows the maximum absorption around 455 nm matching well with the well-known characteristic peak of $[Fe_4S_4(SPh)_4]^{2-}$ (Figure 2E).[17,18]

The zero-field ^{57}Fe Mössbauer spectra also confirm the incorporation of the Fe_4S_4 cluster in the chalcogels for all linking units. The samples ITS-cg1 and ITS-cg3 show similar Mössbauer spectra at 77 K (Figure 3A,B) where the two very closely spaced quadrupole doublets (shown as green and red colored components) suggest a high degree of equivalence among the Fe centers of the clusters in the chalcogels. The

dx.doi.org/10.1021/ja311310k | J. Am. Chem. Soc. 2013, 135, 2330−2337

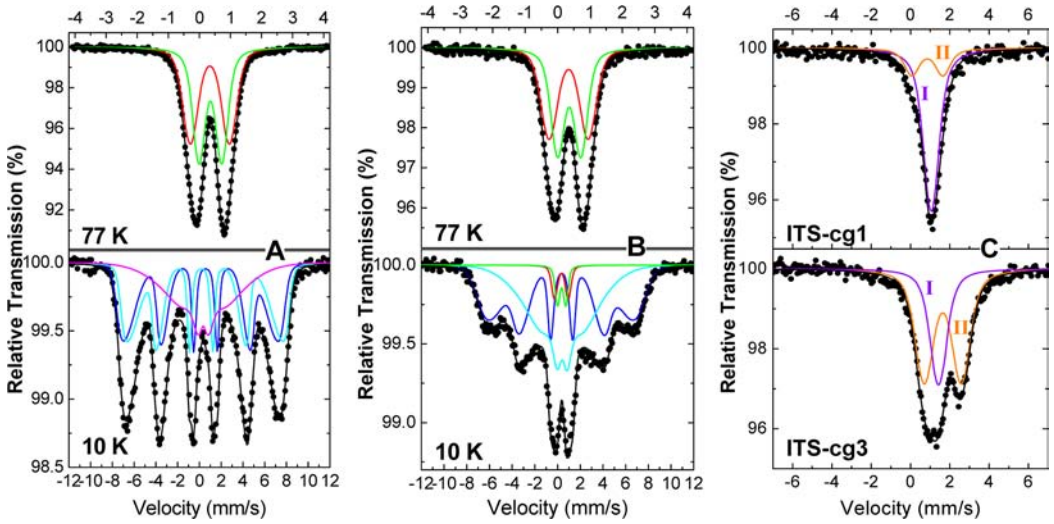

Figure 3. ^{57}Fe Mossbauer spectra of ITS-cg1 (A) and ITS-cg3 (B) recorded at different temperatures. (C) ^{119}Sn Mossbauer spectra of the two samples recorded at 77 K. Experimental data are denoted with points and their deconvolution with the relative components (colored continuous lines explained in the text) is also shown in each spectrum.

Table 3. Mössbauer Data for ITS-cg Series, Isolated Analogous Polycrystalline Fe_4S_4 Complex, and Native Fe_4S_4 Bearing Enzyme

		^{57}Fe		^{119}Sn		
sample	T (K)	δ (mm/s)[a]	ΔE_Q (mm/s)	δ (mm/s)[b]	ΔE_Q (mm/s)	area (%)
ITS-cg1	77	0.44	1.26	1.06	0.26	76
		0.46	0.74	0.86	1.58	24
ITS-cg3	77	0.45	1.21	1.42	0.05	33
		0.47	0.72	1.64	1.89	67
ITS-cg2[c]	40	0.49	1.07	-	-	-
		0.47	0.66			
$(NBu_4)_2[Fe_4S_4(SR)_4]$[d]	100	0.45	1.11	-	-	-
		0.45	0.85			
Ferredoxin from *Clostridium pasteurianum*[e]	77	0.44	1.08	-	-	-

[a]Relative to α-Fe at 300 K. [b]Relative to $BaSnO_3$ at 77 K. [c]Reference 48. [d]Reference 54. [e]Reference 55.

isomer shifts (δ) of the two doublets along with quadrupole splitting parameters match well with previous Mössbauer studies both on isolated, synthetic analogues of Fe_4S_4 cluster and on native Fe_4S_4 cluster bearing proteins (Table 3). The similar δ values are attributed to the same bonding and structure of chalcogels even with different linking units. Therefore, the local environments around the Fe_4S_4 core structure remain uniform in the chalcogels.

At 10 K, the zero-field Mössbauer spectra of both ITS-cg1 and ITS-cg3 show magnetic splitting similar to ITS-cg2[48] (Figure 3A,B). The magnetic splitting at lower temperature seems to be a general characteristic of the biomimetic chalcogel samples, as a consequence of the close spatial proximity of the Fe_4S_4 units in the $[Fe_4S_4]_x[Sn_nS_{2n+2}]_y$ assemblies that results in strong intercubane cluster magnetic coupling. Interestingly, the overall size and charge density of the $[Sn_nS_{2n+2}]^{4-}$ linking blocks seems to scale with the strength of the magnetic coupling experienced between the Fe_4S_4 cubanes in the $[Fe_4S_4]_x[Sn_nS_{2n+2}]_y$ framework. For the ITS-cg3 chalcogel, which contains the larger sized $[Sn_4S_{10}]^{4-}$ linking blocks, the Fe_4S_4 cores are spaced on average farther apart. The hyperfine magnetic fields (B_{hf}) of the two main magnetic components (indicated with blue and cyan colors in Figure 3B) acquire values of 40.2 and 14.8 T, respectively. The spreading of B_{hf} (ΔB_{hf}) for these two components reaches 7.2 and 13.0 T, respectively. The corresponding values at 10 K for the ITS-cg1 chalcogel, which contains the smaller sized $[SnS_4]^{4-}$ units are 45.2 and 45.8 T for B_{hf} and 4.6 and 4.6 T for ΔB_{hf}. In addition, a nonmagnetic ($B_{hf} = 0$) quadrupole split part is detected at the center of the 10 K spectrum of the ITS-cg3 sample (green and red colored components in Figure 3B), while the corresponding center of the 10 K spectrum for the ITS-cg1 sample contains a magnetically split component (magenta colored in Figure 3A) with $B_{hf} = 15.8$ T and $\Delta B_{hf} = 15.2$ T. The higher B_{hf} and lower ΔB_{hf} values found for the 10 K spectral components of ITS-cg1 relative to those of ITS-cg3 denote stronger magnetic coupling between the iron ions of the Fe_4S_4 cubanes in ITS-cg1. This result is a consequence of the enhanced mutual spatial proximity of the Fe_4S_4 cubanes in the ITS-cg1 chalcogel relative to the ITS-cg3 chalcogel. Although these results give only a qualitative view of the magnetic couplings between the Fe_4S_4 units (complete Mössbauer spectra analysis and details for the nature of these couplings is to be reported soon), they certainly reflect an important trend of increasing average Fe_4S_4/Fe_4S_4 separation with increasing size of $[Sn_nS_{2n+2}]^{4-}$ linking blocks which act as spacers in these chalcogels.

The effect of linking blocks is also observed in the zero-field ^{119}Sn Mössbauer spectra of the ITS-cg1 and ITS-cg3 collected at 77 K, providing information on the state of the Sn ions. The

dx.doi.org/10.1021/ja311310k | J. Am. Chem. Soc. 2013, 135, 2330−2337

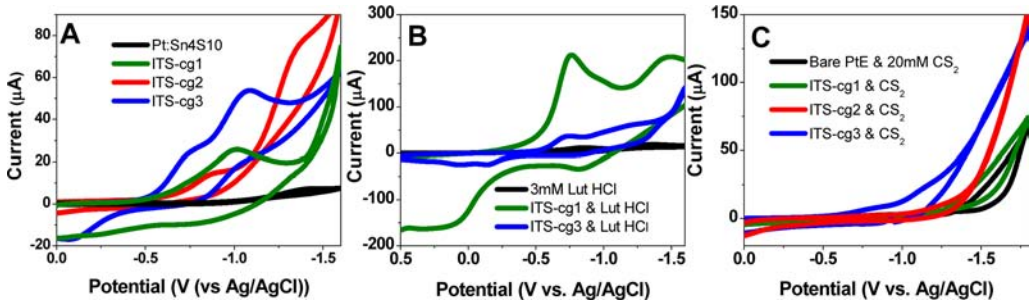

Figure 4. (A) CVs of chalcogels scanned at 60 mV/s; showing redox activity in ITS-cg samples and more anodic reduction potential from ITS-cg1 to ITS-cg3. Pt:Sn_4S_{10} represents a control gel where Pt^{2+} replace Fe_4S_4 centers. (B and C) CVs of ITS-cg with lutidinium chloride (B) and CS_2 (C) as substrates dissolved in solution with scan rate of 60 mV/s.

analysis of each spectrum was done using two components, one with low ΔE_Q (I, violet colored in Figure 3C) and one with high ΔE_Q (II, orange colored in Figure 3C) values. The δ values for all components are characteristic for Sn^{4+} ion as expected for the nature of these ions in the $[Sn_nS_{2n+2}]^{4-}$ linking blocks (Table 3).[39,40] The ΔE_Q values of component II is higher in the ITS-cg3 than in the ITS-cg1, with higher relative absorption area as well (Figure 3C, Table 3). These results suggest that in the chalcogels the Sn^{4+} ions are held in two different environments, one of which (component II) is more distorted than the other (component I). Thus ITS-cg3 chalcogel appears to contain a larger number of Sn^{4+} ions in the distorted environment than ITS-cg1 chalcogel. This could result from the larger number of Sn and S ions accommodated in the $[Sn_nS_{2n+2}]^{4-}$ linking blocks for ITS-cg3, which consequently distort their coordination environment to a higher degree than in ITS-cg1.

The trend observed in the ^{57}Fe Mössbauer spectra regarding the magnetic coupling of the Fe_4S_4 units suggests that the framework of $[Fe_4S_4]_x[Sn_nS_{2n+2}]_y$ in ITS-cg1 are more "dense" and "symmetric" than in ITS-cg3. The latter should contain on average wider spaces defined by the Fe_4S_4 and $[Sn_4S_{10}]^{4-}$ linking blocks and is consistent with the ability for ITS-cg3 to fit a larger number of light harvesting $Ru(bpy)_3^{2+}$ molecules (Table 1), facilitating the photochemical proton reduction experiments (vide infra). The ^{57}Fe and ^{119}Sn Mössbauer spectra suggest that the structure and nature of the Fe_4S_4 units is not affected by the difference in the $[Sn_nS_{2n+2}]^{4-}$ building blocks; however, their average proximity is dictated by the size of the thiostannate anions.

The incorporated Fe_4S_4 units retain their redox activity when the chalcogels are examined with cyclic voltammetry (CV). Using the ITS-cg1, 2, and 3 samples, a CV sweep of potential in the reductive direction shows an initial current wave, corresponding to $[Fe_4S_4]^{2+/+}$ core cluster reduction, near 1000, 870, and 750 mV (vs Ag/AgCl), respectively (Figure 4A). These are associated with cluster reductions and indicate that the clusters are redox switchable. The varying electron densities of the redox-inactive thiostannate units could explain the systematic shifting in reduction potential of the Fe_4S_4 centers. As the charge density of $[Sn_nS_{2n+2}]^{4-}$ decreases from ITS-cg1 to 3, due to increasing size, the reduction potential shifts more anodically. The decreased electron density of $[Sn_4S_{10}]^{4-}$ could make it the least electron-donating group, which results in a more positive Fe_4S_4 reduction potential compared to $[SnS_4]^{4-}$. The CV redox trends are consistent with the Mössbauer spectroscopy results which suggest that *inter*cluster interactions in the Fe_4S_4–Sn_nS_{2n+2} network are the strongest in ITS-cg1 ($[SnS_4]^{4-}$ units) and the weakest in ITS-cg3 ($[Sn_4S_{10}]^{4-}$ units).

The redox activity of the Fe_4S_4 clusters retained in the chalcogel structure combined with the chalcogel's high porosity allows for electrocatalytic action. The ITS-cg2 has already been shown to act as an electrocatalyst showing a large increase in the reduction current while anodically shifting the reduction potential when lutidinium ions or carbon disulfide are used.[48] When the linking units are $[SnS_4]^{4-}$ or $[Sn_4S_{10}]^{4-}$, the chalcogels exhibit different electrocatalytic ability that correlates with their charge density.

In the case of electrochemical reduction of the protons of the lutidinium cations in acetonitrile, all chalcogels exhibit a lowering of the overpotential. The ITS-cg1 shows the most current increase (~20-fold) in addition to the anodic shift in reduction potential (~100 mV) compared to the one observed with the absence of chalcogels on the electrode (Figure 4B). This current increase is much greater than the ~6-fold and ~3-fold current increase observed with ITS-cg2 and 3, respectively.[48]

For the reduction of CS_2, both ITS-cg2 and 3 produce increased current by ~2-fold compared to ITS-cg1 or a bare electrode. In addition, all chalcogels shift the reduction potential to less negative values (Figure 4C). The larger the thiostannate anion, the greater the anodic shift in reduction potential: ~500 mV for ITS-cg3, ~230 mV for ITS-cg2 and ~120 mV for ITS-cg1 (Figure 4C). Therefore, ITS-cg3 reduces the CS_2 at the lowest potential. These electrochemical experiments not only suggest that the chalcogels could be effective electrocatalysts but also can be tuned for suitable substrates relevant to solar fuels.

As mentioned earlier, the existence of the counter cations (Na^+, Ph_4P^+, or $[(CH_3CH_2)_4N]^+$) in the chalcogel framework enables ion exchange and provides a facile route to introducing cationic functional groups. This includes the light harvesting molecule $Ru(bpy)_3^{2+}$(Scheme 1). The presence of $Ru(bpy)_3^{2+}$ in ITS-cg1 and 3 and was confirmed by FTIR spectroscopy and EDS analysis (Supporting Information, Figure S4, Table 1).

The interaction between excited $Ru(bpy)_3^{2+}$ and the anionic network structure was explored by transient absorption spectroscopy (TA). For these experiments, the functionalized chalcogels were sonicated in *o*-dichlorobenzene to give a slurry paste, which was then spuncast onto a glass slide to give a thin film of the chalcogels. All ITS-cg samples, and $Ru(bpy)_3^{2+}$ in solution show the ground state bleaching of $Ru(bpy_3)^{2+}$ at 470 nm (Supporting Information, Figure S5). However, the lifetime of the $Ru(bpy)_3^{2+}$ excited state at 470 nm is clearly shorter in the ITS-cg series (11–28 ns) than in solution (225 ns)

dx.doi.org/10.1021/ja311310k | *J. Am. Chem. Soc.* 2013, 135, 2330–2337

(Supporting Information, Figure S5). As we reported previously, chalcogels functionalized with $Ru(bpy)_3^{2+}$, but lacking the Fe_4S_4 center, exhibit an emissive feature at 620 nm and lack the rapid decay at 460 nm.[48] The emissive feature at 620 nm is only present in $Ru(bpy)_3^{2+}$ solutions and in the gels lacking Fe_4S_4 center, but is not observed in the ITS-cg series of samples (Supporting Information, Figure S5). Therefore, the rapid decay at 470 nm combined with the absence of the 620 nm feature in the ITS-cg series, imply that a different deactivation pathway is possible, presumably involving the Fe_4S_4 centers.[48] In addition, the ground state bleaching lives longer in ITS-cg3 than in ITS-cg1 and 2, suggesting the charge-separated-state is more favored in ITS-cg3 sample (Figure 5).

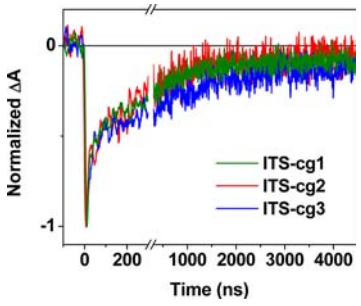

Figure 5. Normalized nanosecond transient absorption at 470 nm of ITS-cg series. The ground state bleaching is the longest in ITS-cg3, indicating a longer charge-separated state in the sample.

The electrochemical and photophysical experiments, suggest that an oxidative quenching of the excited $Ru(bpy)_3^{2+}$ by the Fe_4S_4 clusters is most favored by ITS-cg3 and least favored by ITS-cg1. This leads to the proposed energy level diagram of ITS-cg series and $Ru(bpy)_3$, shown in Figure 6 where the

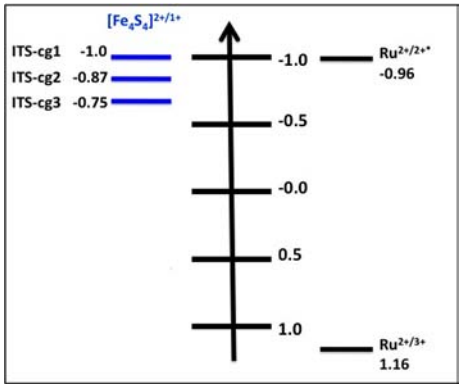

Figure 6. Proposed energy diagram for the $Ru(bpy)_3^{2+}$ in the ITS-cg series. The energy gradient between $[Fe_4S_4]^{2+/1+}$ and $Ru(bpy)_3^{2+/2+*}$ increases from ITS-cg1 to 3.

greatest driving force for energy transfer is with the ITS-cg3. On the contrary, the quenching of excited $Ru(bpy)_3^{2+}$ in the oxidative pathway could be limited in ITS-cg1, and the reductive pathway is rather preferred, contributing to the feature at 505 nm at the TA spectra (Supporting Information, Figure S5). The observed results are consistent with significant oxidative quenching of $Ru(bpy)_3^{2+}$ by the Fe_4S_4 cluster in ITS-cg2 and 3 and limited quenching in ITS-cg1.

The calculated free energy for the photodriven electron transfer from the photogenerated metal-to-ligand charge-transfer state of $Ru(bpy)_3^{2+}$ to the Fe_4S_4 cluster also supports the oxidative pathway. Using the simplified Weller equation,[53] ITS-cg3 has a greater free energy change for this process (ΔG= −210 meV) than ITS-cg2 (ΔG= −90 meV), favoring the oxidative quenching of $Ru(bpy)_3^{2+}$. Acknowledging the Coulombic attraction between the negatively charged ITS-cg framework and the cationic $Ru(bpy)_3^{2+}$, we expect this complex to lie in close proximity to an Fe_4S_4 cluster and therefore the electron transfer between the two is viable (Scheme 2).

Scheme 2. Photochemical Response of ITS-cg3

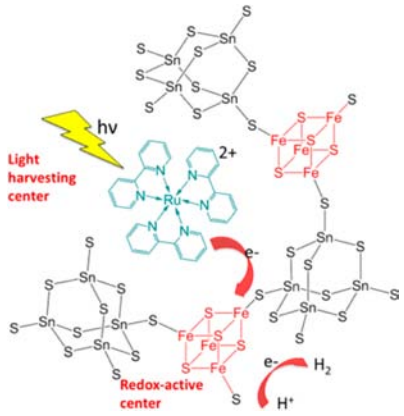

Photochemical proton reduction experiments were performed on the complete ITS-cg series using similar condition as in the previous study.[48] The functionalized chalcogels were placed in an acetonitrile/water (80:20 v/v) solution containing unbalanced molar ratio of lutidinium chloride (50 mM) to sodium ascorbate (10 mM) in order to avoid consuming the lutidinium ions in a possible acid−base reaction with the ascorbate. To help prevent the displacement of the $Ru(bpy)_3^{2+}$ by the lutidinium ions on the surface of the chalcogels we added an excess of $Ru(bpy)_3^{2+}$ (5 mM) into the solvent. After irradiation with a xenon lamp (λ > 300 nm) continuously, H_2 gas was detected by gas chromatography for all chalcogel samples. The amount of H_2 gradually increased over 48 h of illumination and held constant up to the sixth day of illumination (Figure 7). The amount of H_2 evolved seems to reach the "saturation" point after 100 h when the oxygen level in the vial is great enough to deactivate some of Fe_4S_4 centers (Supporting Information, Figure S6). The chalcogel itself did not seem to degrade even after 2 weeks of experiment and did

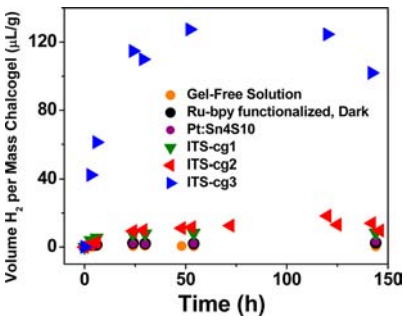

Figure 7. Hydrogen evolution for a variety of chalcogels and conditions. $Pt:Sn_4S_{10}$ represents a control chalcogel where Pt^{2+} replaces the $[Fe_4S_4]^{2+}$ cluster in the structure. The volume of H_2 evolved is normalized to the dry mass of the chalcogels.

dx.doi.org/10.1021/ja311310k | J. Am. Chem. Soc. 2013, 135, 2330−2337

not show any color change, which typically is seen as a sign of oxidation of the Fe_4S_4 clusters. When the chalcogel was kept in dark for a week and then illuminated, the chalcogel started producing hydrogen, which illustrates the stability of our chalcogels in the system. Presumably atmospheric oxygen gradually enters the system (while some hydrogen leaks out) due to the limitations in the experiment apparatus used. Nevertheless, the amount of H_2 gas generated by each chalcogel corresponds to the trend observed in the reduction potentials of $[Fe_4S_4]^{2+/+}$. ITS-cg3 generated the greatest amount of hydrogen (~4-fold increase compared to ITS-cg1) consistent with the most anodic reduction potential of $[Fe_4S_4]^{2+/+}$ (Figure 7). On the contrary, ITS-cg1 produced the least amount of H_2. A longer lifetime of the charge-separated state implied by a longer lived ground state bleaching in ITS-cg3, could contribute to a more efficient electron transfer between the light harvesting system and the redox center in this sample. As proposed by the energy level diagram in Figure 6, the Fe_4S_4 clusters in ITS-cg3 can oxidize the excited $Ru(bpy)_3^{2+}$ more effectively than ITS-cg1 and 2, and therefore, reduce protons to hydrogen most efficiently (Scheme 2).

Although the overall hydrogen evolution is still small, the enhancement is achieved relatively easily by controlling the bridging of the Fe_4S_4 clusters through the different thiostannate linking units. While controlling the ability of the cluster to be reduced electrochemically and photochemically is challenging in the solid-state, the ITS-cg series shows that control can be accomplished in a bottom-up assembly process using a series of thiostannate building blocks with systematically varying the anionic charge density.

CONCLUSION

The ITS-cg series of biomimetic chalcogels presents a novel and simple avenue to tailor the electrochemical and photochemical properties of biomimetic chalcogels for desired solar energy conversion reactions. The $[SnS_4]^{4-}$ and $[Sn_4S_{10}]^{4-}$ building blocks make highly porous frameworks with the Fe_4S_4 clusters stably incorporated. These thiostannate anions result in different bonding interactions with the Fe_4S_4 clusters in the chalcogel structure, affecting the redox activity and modulating its interaction with the excited state of the light harvesting antennae. The tuning ability of these building blocks affects both the quenching of the excited states of the light harvesting antennae and the charge-separated states between the Fe_4S_4 cluster and antennae, leading to an enhancement in photochemical hydrogen production.

The thiostannate blocks do not alter the local environment around one Fe_4S_4 cluster unit; however, their different electron densities affect the charge density on the clusters and the *inter*-cluster interactions, resulting in different reduction potentials of the clusters. These building blocks provide a path to control the electrochemical properties of these chalcogels and can enhance the electrocatalytic and photochemical activity, as seen in the reduction of lutidinium hydrochloride ion, carbon disulfide and protons. The ability to tune the properties of biomimetic chalcogels in a self-assembling polymeric porous system is an important advance in the synthesis of multifunctional materials suitable for a wide range of electrochemical or photodriven catalytic processes involved in solar energy utilization.

ASSOCIATED CONTENT

Supporting Information

Detailed synthesis procedures, experimental procedures, and characterization techniques of chalcogels are presented. The characterization of the precursors and chalcogels (EDS, XRD pattern, UV/vis spectra or Mossbauer spectra) of precursors and chalcogels, FTIR spectra of dye-functionalized gels, and nanosecond transient absorption spectra are included. This material is available free of charge via the Internet at http://pubs.acs.org.

AUTHOR INFORMATION

Corresponding Author

m-kanatzidis@northwestern.edu

Notes

The authors declare no competing financial interest.

ACKNOWLEDGMENTS

We thank Prof. Joseph Hupp for use of the potentiostat. Electron microscopy and elemental analysis were done at the Electron Probe Instrumentation Center at Northwestern University. This research was supported as part of the ANSER Center, an Energy Frontier Research Center funded by the U.S Department of Energy, Office of Science, Office of Basic Energy Sciences, under Award No. DE-SC0001059.

REFERENCES

(1) Barber, J. *Chem. Soc. Rev.* **2009**, *38*, 185.
(2) McConnell, I.; Li, G. H.; Brudvig, G. W. *Chem. Biol.* **2010**, *17*, 434.
(3) Des Marais, D. J. *Science* **2000**, *289*, 1703.
(4) Wasielewski, M. R. *Chem. Rev.* **1992**, *92*, 435.
(5) Nelson, N.; Yocum, C. F. In *Annual Review of Plant Biology*; Annual Reviews: Palo Alto, CA, 2006; Vol. *57*, p 521.
(6) Gust, D.; Moore, T. A.; Moore, A. L. *Acc. Chem. Res.* **2009**, *42*, 1890.
(7) Nelson, N.; Ben-Shem, A. *Nat. Rev. Mol. Cell Biol.* **2004**, *5*, 971.
(8) Kanan, M. W.; Nocera, D. G. *Science* **2008**, *321*, 1072.
(9) Andreiadis, E. S.; Chavarot-Kerlidou, M.; Fontecave, M.; Artero, V. *Photochem. Photobiol.* **2011**, *87*, 946.
(10) Fukuzumi, S. *Phys. Chem. Chem. Phys.* **2008**, *10*, 2283.
(11) Benniston, A. C.; Harriman, A. *Mater. Today* **2008**, *11*, 26.
(12) Gust, D.; Moore, T. A.; Moore, A. L. *Acc. Chem. Res.* **2001**, *34*, 40.
(13) Moore, G. F.; Hambourger, M.; Gervaldo, M.; Poluektov, O. G.; Rajh, T.; Gust, D.; Moore, T. A.; Moore, A. L. *J. Am. Chem. Soc.* **2008**, *130*, 10466.
(14) Meyer, T. J. *Acc. Chem. Res.* **1989**, *22*, 163.
(15) Wasielewski, M. R. *Acc. Chem. Res.* **2009**, *42*, 1910.
(16) Henderson, R. A. *Chem. Rev.* **2005**, *105*, 2365.
(17) Wong, G. B.; Bobrik, M. A.; Holm, R. H. *Inorg. Chem.* **1978**, *17*, 578.
(18) (a) Coucouvanis, D.; Kanatzidis, M.; Simhon, E.; Baenziger, N. C. *J. Am. Chem. Soc.* **1982**, *104*, 1874. (b) Coucouvanis, D.; Kanatzidis, M. G.; Dunham, W. R.; Hagen, W. R. *J. Am. Chem. Soc.* **1984**, *106*, 7998.
(19) Seino, H.; Hidai, M. *Chem. Sci.* **2011**, *2*, 847.
(20) Beinert, H.; Holm, R. H.; Munck, E. *Science* **1997**, *277*, 653.
(21) Zhou, C. Y.; Raebiger, J. W.; Segal, B. M.; Holm, R. H. *Inorg. Chim. Acta* **2000**, *300*, 892.
(22) Kambayashi, H.; Nagao, H.; Tanaka, K.; Nakamoto, M.; Peng, S. M. *Inorg. Chim. Acta* **1993**, *209*, 143.
(23) Osullivan, T.; Millar, M. M. *J. Am. Chem. Soc.* **1985**, *107*, 4096.
(24) Ueyama, N.; Oku, H.; Nakamura, A. *J. Mol. Catal.* **1992**, *74*, 451.

(25) Backes, G.; Mino, Y.; Loehr, T. M.; Meyer, T. E.; Cusanovich, M. A.; Sweeney, W. V.; Adman, E. T.; Sandersloehr, J. *J. Am. Chem. Soc.* **1991**, *113*, 2055.
(26) Johnson, M. K. *Curr. Opin. Chem. Biol.* **1998**, *2*, 173.
(27) Bian, S. M.; Cowan, J. A. *Coord. Chem. Rev.* **1999**, *192*, 1049.
(28) Holm, R. H.; Kennepohl, P.; Solomon, E. I. *Chem. Rev.* **1996**, *96*, 2239.
(29) Doukov, T. I.; Iverson, T. M.; Seravalli, J.; Ragsdale, S. W.; Drennan, C. L. *Science* **2002**, *298*, 567.
(30) Crane, B. R.; Siegel, L. M.; Getzoff, E. D. *Science* **1995**, *270*, 59.
(31) Peters, J. W.; Lanzilotta, W. N.; Lemon, B. J.; Seefeldt, L. C. *Science* **1998**, *282*, 1853.
(32) Allakhverdiev, S. I.; Kreslavski, V. D.; Thavasi, V.; Zharmukhamedov, S. K.; Klimov, V. V.; Nagata, T.; Nishihara, H.; Ramakrishna, S. *Photochem. Photobiol. Sci.* **2009**, *8*, 148.
(33) Carter, C. W. *Iron-Sulfur Proteins*; Academic Press: New York, 1973; Vol. 3.
(34) Tomohiro, T.; Uoto, K.; Okuno, H. *J. Chem. Soc., Chem. Commun.* **1990**, 194.
(35) Gronberg, K. L. C.; Henderson, R. A.; Oglieve, K. E. *J. Chem. Soc., Dalton Trans.* **1998**, 3093.
(36) Sharma, A. K.; Kim, N.; Cameron, C. S.; Lyndon, M.; Gorman, C. B. *Inorg. Chem.* **2010**, *49*, 5072.
(37) Yamamura, T.; Christou, G.; Holm, R. H. *Inorg. Chem.* **1983**, *22*, 939.
(38) Lubner, C. E.; Knorzer, P.; Silva, P. J. N.; Vincent, K. A.; Happe, T.; Bryant, D. A.; Golbeck, J. H. *Biochemistry* **2010**, *49*, 10264.
(39) Gloaguen, F.; Lawrence, J. D.; Rauchfuss, T. B. *J. Am. Chem. Soc.* **2001**, *123*, 9476.
(40) Tye, J. W.; Hall, M. B.; Darensbourg, M. Y. *Proc. Natl. Acad. Sci. U.S.A.* **2005**, *102*, 16911.
(41) Evans, D. J.; Pickett, C. J. *Chem. Soc. Rev.* **2003**, *32*, 268.
(42) Liu, X. M.; Ibrahim, S. K.; Tard, C.; Pickett, C. J. *Coord. Chem. Rev.* **2005**, *249*, 1641.
(43) Tard, C.; Liu, X. M.; Hughes, D. L.; Pickett, C. J. *Chem. Commun.* **2005**, 133.
(44) Wang, W. G.; Rauchfuss, T. B.; Bertini, L.; Zampella, G. *J. Am. Chem. Soc.* **2012**, *134*, 4525.
(45) Wang, F.; Wang, W. G.; Wang, H. Y.; Si, G.; Tung, C. H.; Wu, L. Z. *ACS Catal.* **2012**, *2*, 407.
(46) Schmidt, M.; Contakes, S. M.; Rauchfuss, T. B. *J. Am. Chem. Soc.* **1999**, *121*, 9736.
(47) Ihara, M.; Nishihara, H.; Yoon, K. S.; Lenz, O.; Friedrich, B.; Nakamoto, H.; Kojima, K.; Honma, D.; Kamachi, T.; Okura, I. *Photochem. Photobiol.* **2006**, *82*, 676.
(48) Yuhas, B. D.; Smeigh, A. L.; Samuel, A. P. S.; Shim, Y.; Bag, S.; Douvalis, A. P.; Wasielewski, M. R.; Kanatzidis, M. G. *J. Am. Chem. Soc.* **2011**, *133*, 7252.
(49) Yuhas, B. D.; Prasittichai, C.; Hupp, J. T.; Kanatzidis, M. G. *J. Am. Chem. Soc.* **2011**, *133*, 15854.
(50) Yuhas, B. D.; Smeigh, A. L.; Douvalis, A. P.; Wasielewski, M. R.; Kanatzidis, M. G. *J. Am. Chem. Soc.* **2012**, *134*, 10353.
(51) Kanatzidis, M. G.; Coucouvanis, D.; Simopoulos, A.; Kostikas, A.; Papaefthymiou, V. *J. Am. Chem. Soc.* **1985**, *107*, 4925.
(52) Moulis, J. M.; Meyer, J. *Biochemistry* **1982**, *21*, 4762.
(53) Morandeira, A.; Fortage, J.; Edvinsson, T.; Le Pleux, L.; Blart, E.; Boschloo, G.; Hagfeldt, A.; Hanmiarstrom, L.; Dobel, F. *J. Phys. Chem. C* **2008**, *112*, 1721.
(54) Papaefthymiou, V.; Millar, M. M.; Munck, E. *Inorg. Chem.* **1986**, *25*, 3010.
(55) Thompson, C. L.; Johnson, C. E.; Dickson, D. P. E.; Cammack, R.; Hall, D. O.; Weser, U.; Rao, K. K. *Biochem. J.* **1974**, *139*, 97.